

X-ray variability of NGC 3227 and NGC 5506 and the nature of AGN ‘states’

Philip Uttley^{1*} and Ian M. McHardy²

¹*X-ray Astrophysics Laboratory, Code 662, NASA Goddard Space Flight Center, Greenbelt, MD 20771, USA*

²*School of Physics and Astronomy, University of Southampton, Southampton SO17 1BJ*

ABSTRACT

We use X-ray monitoring data obtained over a broad range of time-scales to measure the broadband power spectral density functions (PSDs) of two Seyfert galaxies, the broad line Seyfert 1 NGC 3227 and the Seyfert 2 NGC 5506, which has recently been identified as an obscured Narrow Line Seyfert 1 (NLS 1). Using a Monte-Carlo fitting technique we demonstrate that both PSDs are reminiscent of the PSD of black hole X-ray binaries (BHXRBs) in the high/soft state, and specifically rule out a low/hard state PSD shape in NGC 3227. This result demonstrates that, at least where variability is concerned, broad line Seyferts with hard X-ray spectra (photon index $\Gamma \sim 1.6$) are not simply the analogues of the low/hard state in BHXRBs, and the dichotomy of NLS 1 and broad line Seyferts cannot be simply interpreted in terms of the two states. We show that the PSD normalisation in NGC 3227 is strongly energy dependent, with larger variability amplitudes at lower energies, unlike NGC 5506 which shows little energy-dependence of variability. We demonstrate that this difference is caused by spectral pivoting of the continuum in NGC 3227 at high energies, which is probably also related to the large amplitude of variability seen in the 2–10 keV band in this AGN. Using the new PSD data and new results in the literature, we replot the PSD break time-scale versus mass plot for all AGN with PSD breaks measured so far, and demonstrate that higher accretion-rate AGN appear to have relatively shorter break time-scales for their black hole mass than lower-accretion rate AGN.

Key words: X-rays: galaxies – galaxies: active – galaxies: Seyfert – galaxies: individual: NGC 3227 – galaxies: individual: NGC 5506 – methods: statistical

1 INTRODUCTION

The X-ray variability of radio-quiet active galactic nuclei (AGN) measured to date is best characterised as a red-noise process, with a power-law PSD of slope ~ -2 on short time-scales (hours to days, McHardy 1988; Green, McHardy & Lehto 1993). In the last few years, longer-time-scale monitoring of AGN, on time-scales of weeks to years, with the *Rossi X-ray Timing Explorer (RXTE)* has revealed breaks in the PSDs, with the PSD flattening to slopes ~ -1 below the break frequency (e.g. Edelson & Nandra 1999; Uttley, McHardy & Papadakis 2002; Markowitz et al. 2003; McHardy et al. 2004, 2005), similar to the high-frequency breaks (around 1–10 Hz) observed in the PSDs of black hole X-ray binaries (BHXRBs). Comparison of the break frequencies (or equivalently, time-scales) with independent measures of black hole mass shows that they scale roughly linearly with mass from the time-scales observed in BHXRBs,

albeit with some scatter (Markowitz et al., 2003; McHardy et al., 2004). This remarkable connection with the X-ray variability properties of stellar mass black-holes raises the possibility that other properties of these sources are similar. For example, since BHXRBs show a range of states with different X-ray spectral and variability properties (see McClintock & Remillard 2005 for a review), we can ask, do AGN show a similar range of states?

Narrow Line Seyfert 1 (NLS 1) are often compared with BHXRBs in the high/soft state or very high states, since they show steep power-law X-ray spectra $\Gamma > 2$ (Brandt, Mathur & Elvis, 1997), similar to the steep power-laws observed in the high/soft state of BHXRBs[†]. On the other hand, broad line Seyfert galaxies have harder X-ray spec-

[†] BHXRBs in the high/soft state also show strong disk blackbody emission at temperatures $kT \sim 1$ keV, which would generally not be observed in the X-ray spectra of AGN, due to their lower disk temperatures

* e-mail: pu@milkyway.gsfc.nasa.gov

tra ($\Gamma < 2$) and so have been compared with BHXRBs in the low/hard state. This dichotomy is also reflected in the X-ray variability of NLS 1 and broad line AGN, with high-luminosity NLS 1 showing typically larger variability on short time-scales (hours) compared to broad line Seyferts, which show weaker variability with increasing luminosity (Turner et al., 1999; Leighly, 1999). Comparison of PSD break time-scales with independent estimates of black hole mass suggested that this difference in variability amplitude may be due to a systematically shorter break time-scale in the PSDs of NLS 1 (M^cHardy et al., 2004), consistent with the interpretation that NLS 1 occupy the high/soft state, which shows a higher PSD break frequency than the low/hard state ($\sim 10 - 20$ Hz versus \sim few Hz). More recently, using the latest revised estimates of black hole masses M^cHardy et al. (2005) have shown that the break time-scales of broad line Seyferts are consistent with scaling from the high/soft state, in which case the relative difference in break time-scales may reflect a more gradual dependence of time-scale on e.g. accretion rate, rather than a sharp transition between high/soft and low/hard accretion states (see also Markowitz & Uttley 2005). It is not clear if the normalisations of NLS 1 PSDs are also systematically higher than those of broad line Seyferts. The comparison with BHXRBs is more complicated here, since only the power-law continuum is significantly variable in high/soft state BHXRBs (Churazov, Gilfanov & Revnivtsev, 2001) so the amplitude of variability (i.e. PSD normalisation) is reduced by the presence of the constant blackbody which would not be observed in AGN.

A more clear-cut test of the existence of different states in AGN is the shape of the broadband PSD. This is because the low/hard and high/soft states in BHXRBs show a clear and simple difference in PSD shape. High/soft state PSDs show power continuing below the break with an unbroken power-law slope ~ -1 down to very low frequencies ($< 10^{-3}$ Hz, Reig, Papadakis & Kylafis 2002). On the other hand, low/hard state PSDs show a second break: a cut off in the power (to slope 0) below ~ 0.1 Hz, so that there is only significant power over about a decade range in frequency (Belloni & Hasinger, 1990; Pottschmidt et al., 2003). The best evidence for a low/hard state PSD shape in an AGN has been obtained for the broad line Seyfert 1 NGC 3783 (Markowitz et al., 2003); although the precise low-frequency shape is unclear, the PSD does appear to flatten and is not consistent with an unbroken slope of -1 at the 98 per cent confidence level. In contrast, the best-quality broadband AGN PSD measured to date is for the NLS 1 NGC 4051, which clearly showed a continuation of power to low frequencies with slope ~ -1.1 over a > 3 -decade range, consistent with a high/soft state interpretation. A similar result is also obtained for MCG-6-30-15 (M^cHardy et al., 2005).

In this paper, we present the broadband PSD of a broad line Seyfert 1.5, NGC 3227 [‡], which shows that this AGN

[‡] Although the FWHM of H β emission in the mean spectrum is only 1900 km s⁻¹ (hence the Seyfert 1.5 classification) this is probably due to contamination by a constant narrow emission line, since the FWHM of the H β line in the rms-spectrum is ~ 4300 km s⁻¹ (Onken et al., 2003).

has a high/soft state PSD shape despite possessing an intrinsically hard X-ray continuum ($\Gamma \sim 1.6$,) and an apparently low accretion rate (few per cent Eddington). We also show that the PSD of the Seyfert 2 NGC 5506, recently identified as an obscured NLS 1 (Nagar et al., 2002) is consistent with a high/soft state shape, but has significantly lower normalisation than the PSD of NGC 3227. Both AGN also show different energy dependences of the PSD normalisation, with NGC 3227 showing increasing amplitude of variability at lower energies while NGC 5506 shows little energy dependence of variability. In combination, these results show that the high/soft and low/hard state dichotomy cannot be simply applied to describing NLS 1 and broad line Seyferts, at least in regard to their variability properties.

2 OBSERVATIONS AND DATA REDUCTION

We have monitored NGC 3227 from 1999 Jan 2 to the present (data obtained up to 2005 Feb 24 is used here), and NGC 5506 from 1996 Apr 23 to 2002 May 20 as part of our program to measure the broadband PSDs of AGN. In order to efficiently sample variability over a broad range of time-scales, we observe our targets using 1 ksec snapshots with the Proportional Counter Array, which are obtained over a range of (roughly evenly-spaced) sampling intervals. Until the end of 2000 February, *RXTE* observed the sources using a combination of twice-daily, daily, bi-weekly and also monthly monitoring (see Uttley, M^cHardy & Papadakis 2002, henceforth UMP02, for PSDs of several AGN, including NGC 5506, constructed using this data). From 2000 March to 2001 February, *RXTE* carried out weekly observations, and also carried out intensive 4-times-daily monitoring of each AGN for two months, in order to better constrain the PSD on intermediate time-scales. Then, from 2001 March to 2002 February (for NGC 5506), and up until the present in the case of NGC 3227, the sampling rate of long-term monitoring increased to every two days, in order to better pin down the lower-frequency shape of the PSD, which is heavily influenced by aliasing from higher frequencies (e.g. see UMP02).

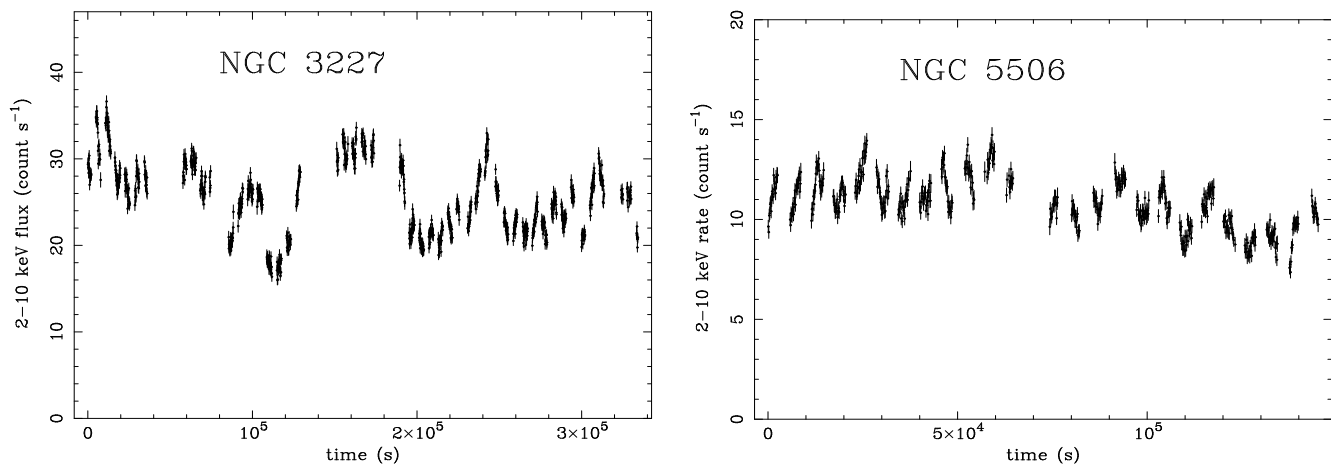
In order to constrain the short-term variability and measure the PSD at high frequencies, we use long-look observations, of \sim days duration. For NGC 3227, we obtained an archival *RXTE* observation of ~ 4 d duration. For NGC 5506, as noted in UMP02, our original ‘long-look’ observation was poorly sampled, so that it was only suitable for use in measuring the PSD at relatively high frequencies ($> 10^{-4}$ Hz, i.e. time-scales less than an *RXTE* orbit). Therefore in UMP02 we also used an archival long-look observation with the ME instrument on board *EXOSAT* to constrain the PSD at frequencies 10^{-5} – 10^{-4} Hz, and we also use the same observation here (see UMP02 for further details). However, subsequently a somewhat short (~ 1.7 d) but well-sampled *RXTE* long-look observation (2001 December) has become available, which we also use to constrain the PSD over the same frequency range as the *EXOSAT* data. We summarise the observations used in this paper in Table 1.

We reduce all the PCA data using standard selection criteria (e.g. see M^cHardy et al. 2004), using the latest background models and extracting data from the top layer only

Table 1. Lightcurve details

Target	Name	Sampling	Proposal ID	N ^o : Obs/Exposure
NGC 3227	long-look	orbital gaps	10292	125 ks
NGC 3227	daily	28×12h,28×1d	40151	56
NGC 3227	6-hourly	256×6h	50153	237
NGC 3227	long-term	88×1w, 618×2d	40151, 50153, 60133, 70142, 80154, 90160	693
NGC 5506	1997 long-look	irregularly sampled	20318	85 ks
NGC 5506	2001 long-look	orbital gaps	60135	69 ks
NGC 5506	<i>EXOSAT</i> long-look	continuous	2021	212 ks
NGC 5506	daily	28×12h,28×1d	10301	47
NGC 5506	6-hourly	256×6h	50153	250
NGC 5506	long-term	14×1m, 53×2w, 43×1w, 183×2d	10301, 20319, 30219, 40151, 50153, 60133	286

The table shows the name of the separate lightcurve used to construct the broadband PSD, the sampling pattern (6h - 6 hourly; 2d - every 2 days; 1w - weekly; 2w - every 2 weeks; 1m - monthly), *RXTE* Proposal IDs containing the data and the number of useful observations (for monitoring) or useful exposure time (for long-looks).


Figure 1. Long-look 2-10 keV *RXTE* light curves of NGC 3227 and NGC 5506.

of the available PCUs. For the long-look data, obtained over short periods so that the instrument response is constant, we measured light curves directly in terms of count rates in the 2-10 keV band[§]. To maximise signal-to-noise in determining the high-frequency PSDs, we extracted data from segments when all 5 PCUs were switched on for the 1996 NGC 3227 and 1997 NGC 5506 long-looks respectively. Since 1999 March, instrumental problems with the PCA instrument have led to losses in the number of typically available Proportional Counter Units ¶, so that we only extract counts from PCU 2 in the 2001 NGC 5506 long-look, to yield a light curve with similar count rate to the *EXOSAT* observation. We plot the NGC 3227 and 2001 NGC 5506 long-look lightcurves in Fig. 1.

The PCU losses, together with significant changes in the PCA voltage gain, mean that it is not possible to simply measure a long-term light curve using the instrument count rate. Therefore, we use a spectral-fitting approach to mea-

sure the observed energy fluxes. We extract the the spectrum from each monitoring snapshot and fit it with a simple absorbed power-law model over the 3-12 keV energy range. The neutral absorbing column is fixed at the estimated Galactic value for the Seyfert 1 NGC 3227 ($N_{\text{H}} = 2.1 \times 10^{20} \text{ cm}^{-2}$, Murphy et al. 1996), and at an assumed intrinsic value of $N_{\text{H}} = 3.6 \times 10^{22} \text{ cm}^{-2}$ for the Seyfert 2 galaxy NGC 5506 (consistent with the results of fits to broadband *BeppoSAX* data, Bianchi et al. 2003). The flux in the 2-10 keV energy range is then determined from the fitted model. Although the model used to fit the data is relatively simple, it serves as a good estimator of the 2-10 keV flux, because the *RXTE* response is relatively flat so that provided the model is a good fit to the data, the integrated flux is a good approximation to the count rate ‘corrected’ for changes in the response and number of PCUs. We plot the resulting long-term and 6-hourly light curves in Fig. 2 and Fig. 3 respectively.

Fitting a better, more detailed spectral model (e.g. including an iron line) is not warranted by the relatively poor statistics of the 1 ks snapshots. We note however that since the absorbing column is fixed in our fits, the resulting flux estimates will include any variations due to absorption. In NGC 5506, we do not expect such changes in absorbing column, since there is good evidence that the Compton-thin column in this case is due to large-scale absorption in the plane of the edge-on host galaxy (Nagar et al., 2002; Bianchi et al., 2003). In NGC 3227 however, the *RXTE* monitoring

[§] instrument channels 5-27 in the long-looks obtained before the 1999 Mar gain change, channels 5-24 in the NGC 5506 long-look obtained in 2001 Dec.

¶ PCUs 1,3 and 4 are often switched off to prevent their degradation, and since PCU 0 suffers substantially higher background due to the loss of its Propane veto layer, we typically only use data from PCU 2 from observations obtained since 2000.

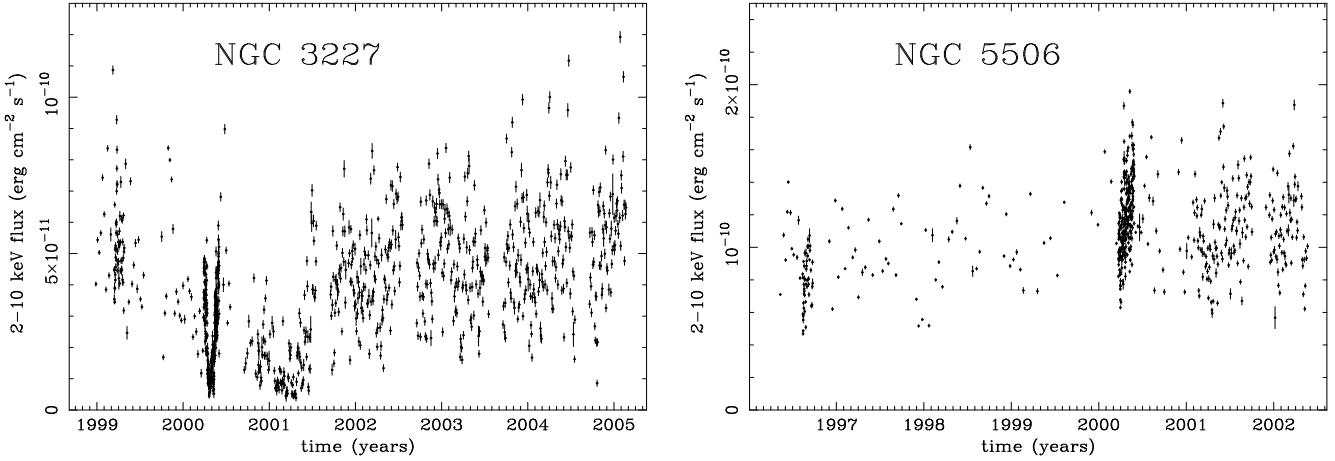


Figure 2. Long-term 2-10 keV flux light curves of NGC 3227 and NGC 5506.

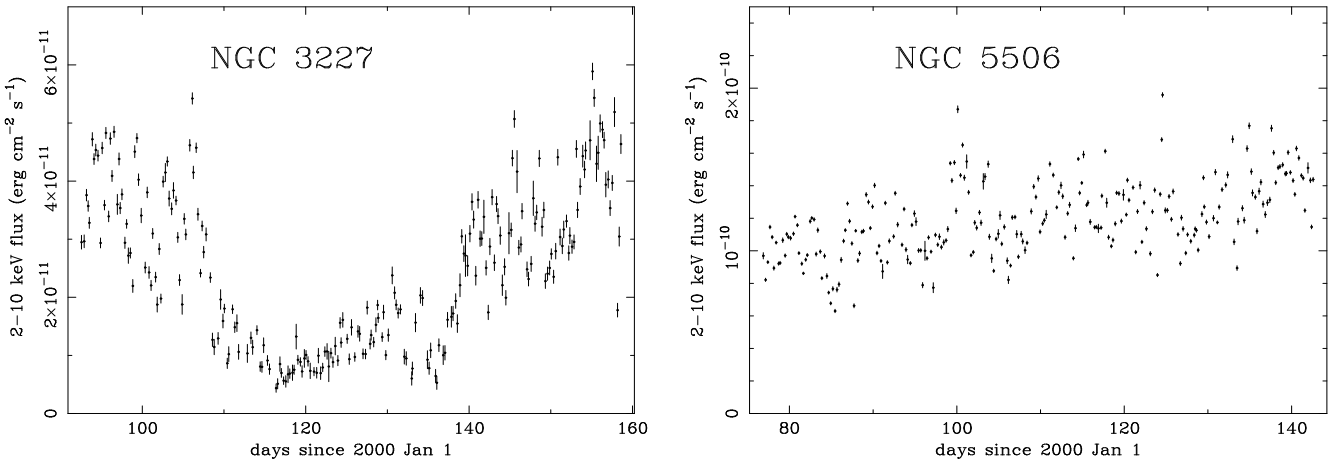


Figure 3. 6-hourly 2-10 keV flux light curves of NGC 3227 and NGC 5506.

has revealed an absorption event of several months duration, when the column increased to $\sim 3 \times 10^{23}$ before returning to the normal low level, possibly as a result of an eclipse of the X-ray source by a Broad Line Region cloud (Lamer, Uttley & McHardy, 2003). We will show that this absorption-related variation has a negligible effect on the measured PSD later in the paper.

3 MONTE-CARLO ANALYSIS

For several reasons, a Monte-Carlo approach is essential to constrain the shape of the PSD measured from monitoring observations of the kind presented here. Firstly, the mixture of sampling patterns means that aliasing and red-noise-leak effects, which systematically distort the PSD, cannot be trivially calculated, so such effects must be accounted for with direct simulation. Secondly, the distorting effects of sampling mean that adjacent frequency bins in the PSD are not independent, so that meaningful errors cannot be derived directly from the data and used with a conventional goodness-of-fit statistic. Thirdly, in order to sample the PSD down to low frequencies and so better constrain the low-frequency shape, it is necessary to minimally bin the PSD at

the lowest frequencies, so that even if sampling effects were negligible, meaningful errors on the PSD could not be determined. These problems (which are discussed in some detail in UMP02 and Vaughan et al. 2003b) mean it is necessary to use a Monte-Carlo approach to fit models to the PSD. In UMP02, we developed a Monte-Carlo approach (called PSRESP, based on the ‘response method’ of Done et al. 1992) to fitting broadband PSD models to data consisting of multiple light curves, sampling a range of time-scales.

The PSRESP method has subsequently been applied to a number of studies of AGN PSDs (Markowitz et al., 2003; McHardy et al., 2004) and we refer the reader to these papers, in addition to UMP02, for further discussion of the method. Here, we simply note some of the technical details of the PSRESP fitting of the data discussed in this paper. The light curves detailed in Table 1 (with the exception of the 2001 NGC 5506 long-look) are used as direct input into PSRESP, which rebins them into time bins of size T_{bin} s. The long-term light curve, used to calculate the low-frequency part of the PSD also includes the more intensely sampled monitoring data (i.e. with 6 h, 12 h and 1 d sampling), but since this light curve contains gaps of 4 or 8 weeks in NGC 5506 and NGC 3227 respectively (due to Sun-angle pointing constraints), we choose a wide bin size

$T_{\text{bin}} = 28$ days, to minimise any unnecessary distortion to the PSD. For the remaining light curves, the data is rebinned to a bin time close to the sampling time-scale: 2048 s for the long-looks, 6 h for the 6-hourly sampled data, and 1 d for the daily and twice-daily monitoring data sets, which are consecutive and hence combined into a single light curve for improved S/N . PSRESP then interpolates any empty bins, and renormalises the light curves by the mean flux before measuring the PSD for each input light curve (the set of PSDs then forms the overall broadband PSD). The PSDs are rebinned in logarithmic frequency intervals $\nu \rightarrow 1.5\nu$, with a minimum of 2 frequencies per bin. To constrain the very highest frequencies $\nu > 10^{-4}$ Hz (close to the Poisson noise level), which do not require extensive simulation since the light curves are continuously sampled on those time-scales less than half an *RXTE* orbit, very high frequency (VHF) PSDs were directly computed from NGC 3227 and 1997 NGC 5506 long-look light curves with 16 s resolution. Error bars on the VHF PSD are determined directly from the data, so that these PSDs are directly input into PSRESP and only red-noise leak in the VHF PSD is accounted for by the code.

Simulated light curves are made using a time resolution $T_{\text{sim}} \leq T_{\text{bin}}/10$ (additional power due to shorter time-scales is estimated using an analytical approximation, see UMP02). As with the real data, PSDs measured from the simulations are rebinned in logarithmic frequency intervals $\nu \rightarrow 1.5\nu$, with a minimum of 2 frequencies per bin. Unless otherwise noted, for each input light curve, $N = 400$ simulations are made for each step of assumed PSD model parameters, and used to determine the model average PSDs and the spread in power at each frequency bin. $M = 4000$ combinations of the simulated PSDs are chosen to make simulated broadband PSDs, and compared with the model average to determine a pseudo- χ^2 distribution, which is used to determine the goodness of fit of the model to the observed broadband PSD.

4 RESULTS

4.1 The 2-10 keV PSD of NGC 3227

We first fitted an unbroken power-law model to the 2-10 keV PSD of NGC 3227, using $N = 1000$ simulated PSDs and $M = 10000$ combinations of PSDs to determine the rejection probability. The model was rejected at better than 99.9 per cent confidence. Examination of the fit residuals clearly shows evidence of spectral flattening towards low-frequencies. However, the long-term data for NGC 3227 (Fig. 2) shows clear evidence for long-time-scale variability, indicative of a red-noise like PSD on long time-scales, so that the PSD must not flatten to zero. By analogy with our previous fit to the PSD of NGC 4051 (M^cHardy et al., 2004), the simplest model may be a bending power-law, similar to that observed in Cyg X-1 in its high/soft state, described by:

$$P(\nu) = A\nu^{\alpha_L} \left(1 + \left(\frac{\nu}{\nu_{\text{bd}}} \right)^{-\alpha_H + \alpha_L} \right)^{-1}$$

Where A is a normalising factor, α_L and α_H denote the low and high frequency slopes respectively and ν_{bd} is the bend

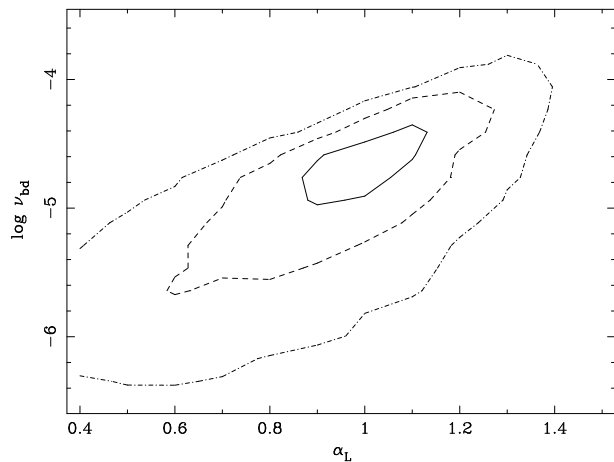


Figure 4. NGC 3227 confidence contours of PSD bend frequency versus low-frequency slope. Solid, dashed and dot-dashed lines denote the 68 per cent, 90 per cent and 99 per cent confidence contours respectively.

frequency. We allowed all parameters in the model to be free and fitted the model to the broadband PSD. The acceptable (at 90 per cent confidence) range of high-frequency slopes is fairly steep, $\alpha_H < -2$ (note that slopes steeper than two cannot be constrained due to the effects of red-noise leak, e.g. see UMP02 for discussion). The acceptable region of the $\nu_{\text{bd}}-\alpha_L$ parameter space is shown in Fig. 4. The best fit (rejection probability $P_{\text{rej}} = 0.54^{\parallel}$) was found for a low-frequency slope $\alpha_L = -1$ and bend-frequency $\nu_{\text{bd}} = 2.6 \times 10^{-5}$ Hz. The data and best-fitting model are plotted in Fig. 5. The fact that the low-frequency slope is similar to -1 is consistent with the shape of the high/soft state PSD in Cyg X-1. It is interesting to compare Fig. 4 with the similar plot for NGC 4051 [Fig. 13 in M^cHardy et al. (2004)]. The low-frequency slope is similar in both cases, while the bend-frequency is more than an order of magnitude lower in NGC 3227, suggesting a similar variability state but a significantly higher-mass black hole in NGC 3227.

Having demonstrated that the broadband PSD of NGC 3227 is consistent with a bending power-law similar to the PSDs of NGC 4051 and Cyg X-1 in the high/soft state, we now consider whether we can rule out the possibility of a low/hard state PSD shape. Although the low/hard state PSD appears to be best-described by a sum of broad Lorentzians (e.g. Nowak 2000; Pottschmidt et al. 2003), a doubly-broken power-law (with sharp breaks, e.g. see Markowitz et al. 2003 Section 4.3) will suffice to represent the shape of the PSD (e.g. see Belloni & Hasinger 1990; Nowak et al. 1999), especially for data of necessarily poorer quality than for XRBs. To mimic the shape of the low/hard state PSD we fix the low and intermediate power-law slopes to 0 and -1 respectively, but allow the high-frequency slope to remain free (since it appears to vary in Cyg X-1, Belloni & Hasinger 1990). We also leave the positions of both the low and high frequency-breaks to be free, in order to de-

^{||} Rejection probability gives the fraction of simulated data sets which are a better fit to the assumed model than the real data, i.e. the confidence that the model is rejected by the data.

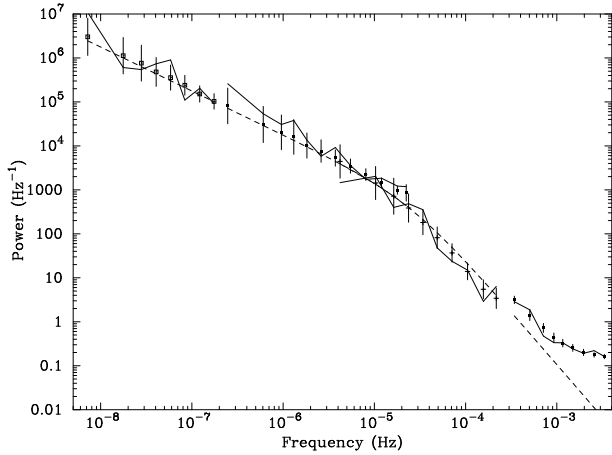


Figure 5. NGC 3227 observed broadband PSD (solid lines) compared with the best-fitting bending power-law model. The underlying model PSD is shown by a dashed line, while the model distorted by sampling as determined by the simulations is shown by data points, with error bars to show the computed spread in observed power at each frequency. The different contributing distorted PSDs are distinguished by different markers. The Poisson noise level has not been subtracted from the data or distorted model. For clarity the PSD produced from daily monitoring (covering $\sim 10^{-6}$ – 10^{-5} Hz) is not shown in the plot.

termine the allowed width of the part of the PSD with the intermediate $1/f$ slope, which is typically about a decade in the low/hard state of BHXRBs.

The resulting contour plot of low-frequency versus high-frequency breaks is shown in Fig. 6. The best-fitting model ($P_{\text{rej}} = 0.59$) corresponds to a low-frequency break of 10^{-8} Hz, on the edge of the fitted range, i.e. the data are consistent with there being no low-frequency break. Importantly, the possible ratio of the high and low break frequencies is greater than 30 at 95 per cent confidence and likely exceeds 100 (at 90 per cent confidence). Therefore the allowed width of the intermediate $1/f$ slope is significantly greater than the decade observed in the low/hard state of BHXRBs, and we rule out a low/hard state interpretation of the PSD. It is much more likely that the PSD of NGC 3227 is similar to that of the high/soft state in BHXRBs.

We stress here that the X-ray absorption event observed in NGC 3227 in late 2000 and early 2001 (Lamer, Uttley & McHardy, 2003) is unlikely to contribute significantly to the long-term PSD. This is because the time when absorption is at a maximum (and hence significantly affects the 2–10 keV flux) corresponds to roughly a single month-long bin (out of more than 70 bins) in the light-curve used to make the PSD. Accordingly, removing this data point and interpolating across the gap, has a negligible effect on our PSD fit results. Furthermore, the X-ray spectral variability of NGC 3227 is consistent with long time-scale variations being due to intrinsic continuum variations and not absorption variations (Lamer, Uttley & McHardy 2003 and see Section 5.2). This result is also supported by similarity of the PSD shapes in the 3–5 keV and 7–15 keV energy bands (see Section 4.3).

For completeness, and a comparison with other results (e.g. Uttley, McHardy & Papadakis 2002; Markowitz et al. 2003), we also fitted a sharply-broken power-law PSD

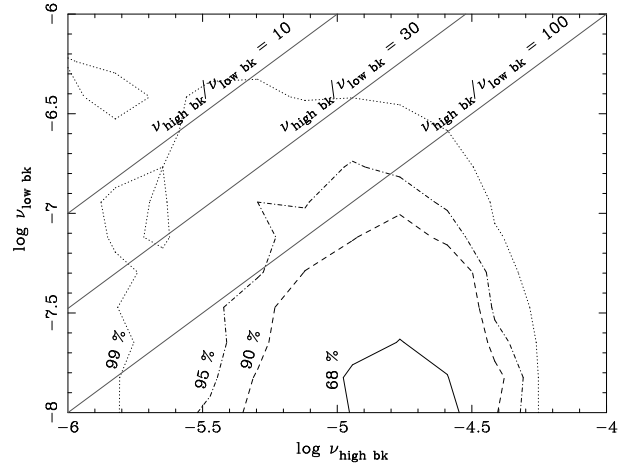


Figure 6. NGC 3227 confidence contours of PSD low-frequency versus high-frequency break for the doubly-broken power-law model. The three solid diagonal lines denote break-frequency ratios of 10, 30 and 100. A ratio of < 30 is ruled out at 95 per cent confidence.

model to the data (with low-frequency slope fixed to -1). We obtain a good fit ($P_{\text{rej}} = 0.54$) for a break frequency of $(1.9 \pm_{1.4}^{2.5} \times 10^{-5}$ Hz (errors are 90 per cent confidence limits here and elsewhere, unless otherwise noted) for high-frequency slopes constrained to be steeper than -1.9 (at 90 per cent confidence).

4.2 The 2–10 keV PSD of NGC 5506

Following the procedure used for NGC 3227, we first fitted an unbroken power-law model to the 2–10 keV PSD of NGC 5506, and find that it is rejected at better than 99.9 per cent confidence (strengthening the 99 per cent confidence result we obtained with fewer data in UMP02), again due to low-frequency flattening. We next fitted the bending power-law model. The high-frequency slope is constrained to be $\alpha_H < -1.7$ (at 90 per cent confidence) and a best fit (rejection probability $P_{\text{rej}} = 0.27$) was found for a low-frequency slope $\alpha_L = -1$ and bend-frequency $\nu_{\text{bd}} = 3.9 \times 10^{-5}$ Hz. The data and best-fitting model are shown in Fig. 7. The data is consistent with a high/soft state PSD shape, with a similar bend frequency to that observed in NGC 3227. However, the low-frequency slope is not very well constrained (see Fig. 8) and hence is also consistent with zero at the 90 per cent confidence limit. Not surprisingly, we find that the doubly broken power-law model is also an acceptable fit to the data (at the 90 per cent confidence level) even for small values (< 10) of the ratio of high to low break frequency. Therefore we cannot rule out the possibility of a low/hard state PSD shape in NGC 5506. A sharply broken power law (with low-frequency slope -1) also produced a good fit to the PSD ($P_{\text{rej}} = 0.44$), for a break frequency $(1.3 \pm_{0.7}^{8.3} \times 10^{-5}$ Hz for slopes steeper than -1.8 (at 90 per cent confidence).

4.3 Energy dependence of PSD shape and normalisation

We now consider the energy dependence of the PSD shape and normalisation for both targets. For the monitoring data,

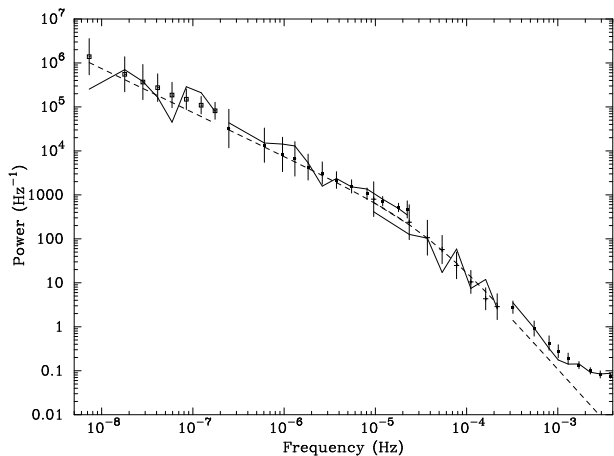


Figure 7. NGC 5506 observed broadband PSD (solid lines) compared with the best-fitting bending power-law model. The underlying model PSD is shown by a dashed line, while the model distorted by sampling as determined by the simulations is shown by data points, with error bars to show the computed spread in observed power at each frequency. The different contributing distorted PSDs are distinguished by different markers. The Poisson noise level has not been subtracted from the data or distorted model. For clarity the PSDs produced from daily monitoring (covering $\sim 10^{-6}$ – 10^{-5} Hz) and the *EXOSAT* data (from $\sim 10^{-5}$ – 10^{-4} Hz) are not shown in the plot.

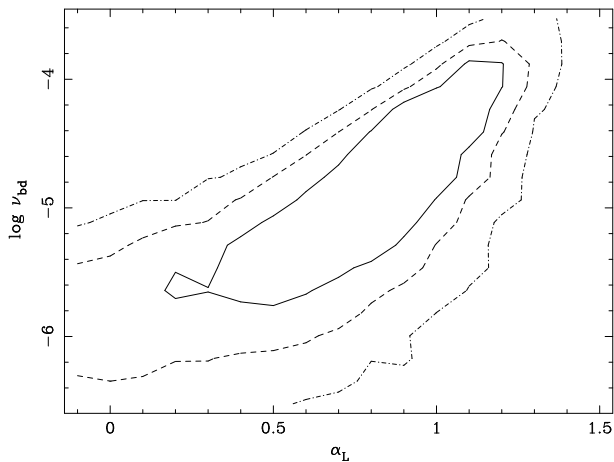


Figure 8. NGC 5506 confidence contours of PSD bend frequency versus low-frequency slope. Solid, dashed and dot-dashed lines denote the 68 per cent, 90 per cent and 99 per cent confidence contours respectively.

we measured flux light curves in two energy bands, 3–5 keV and 7–15 keV, using the spectral-fitting method described in Section 2, except only fitting the spectrum obtained over the respective energy ranges, rather than a broader band. We extracted count-rate light curves for the long-look observations over the equivalent channel ranges^{**}. Since the *EXOSAT* data for NGC 5506 does not extend to energies above 9 keV

^{**} instrument channels 5–13 and 19–41 for 2–5 keV and 7–15 keV bands respectively in the long-looks obtained before the 1999 Mar gain change, channels 5–11 and 17–36 in the NGC 5506 long-look obtained in 2001 Dec. Note that although channel 5 extends to

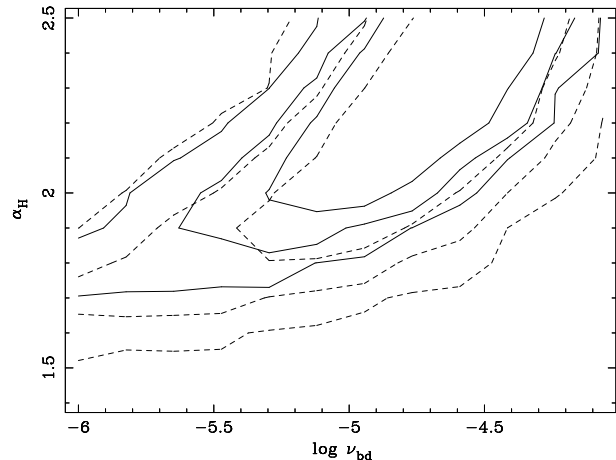


Figure 9. NGC 3227: comparison of confidence contours of PSD bend frequency versus low-frequency slope, for the 3–5 keV PSD (solid lines) and 7–15 keV PSD (dashed lines). Inner to outer contours represent the 68 per cent, 90 per cent and 99 per cent confidence limits respectively.

we do not use that data to make energy-dependent high-frequency PSDs, but continue to use the *RXTE* long-look data from 2001 Dec.

We fit the bend model, which provides a good fit to the PSDs of both AGN, in order to investigate the energy-dependence of the PSD shape. The high-state PSD of Cyg X-1 is energy-independent below the bend-frequency (M^cHardy et al., 2004), so we fix the low-frequency slope to -1 for both AGN, allowing the bend-frequency and high-frequency slope to be free. We show overlaid confidence contour plots for the fits to both energy bands in Fig. 9 and Fig. 10 for NGC 3227 and NGC 5506 respectively. For both sources, the PSDs in both energy bands are consistent with having the same shape. The PSD shapes are also consistent with the shape of the 2–10 keV PSD. Note however, that since the light curves in both bands are fairly well correlated in both sources, the uncertainty in PSD shape is correlated between bands, i.e. although there is an overall systematic uncertainty in PSD shape for both bands the relative difference in shapes is not as large as might be inferred from the size of the confidence contours. With this point in mind, we note a tendency in both AGN for the fits to the 2–5 keV PSD to favour slightly lower bend-frequencies and/or steeper high-frequency slopes, i.e. there is relatively more power at higher frequencies in the harder energy band than in the softer band. Similar behaviour has been more conclusively observed in the PSDs of several other AGN (Nandra & Papadakis, 2001; Vaughan, Fabian & Nandra, 2003a; M^cHardy et al., 2004), although the same behaviour is not observed in Cyg X-1 in the high/soft state (M^cHardy et al., 2004). Better data or a more sophisticated comparison of PSDs in different energy bands are required to conclusively demonstrate this behaviour in our targets.

A more robust comparison can be made between the PSD normalisations in the different energy bands, and between the PSD normalisations of both AGN. In the bending

2 keV the instrument effective area is only small so these energies do not contribute significantly to the count rate.

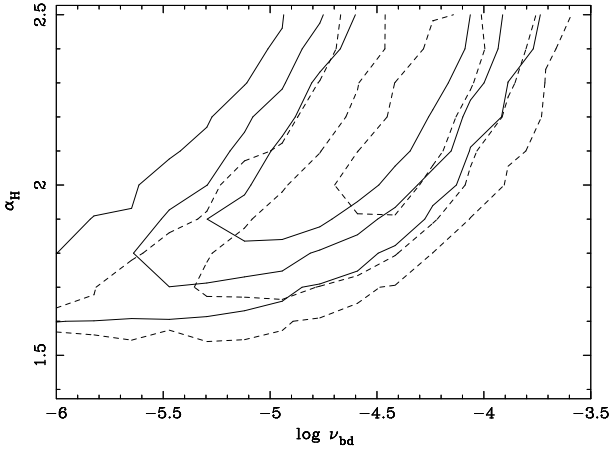


Figure 10. NGC 5506: comparison of confidence contours of PSD bend frequency versus low-frequency slope, for the 3-5 keV PSD (solid lines) and 7-15 keV PSD (dashed lines). Inner to outer contours represent the 68 per cent, 90 per cent and 99 per cent confidence limits respectively.

Table 2. PSD normalisations and fractional rms of long-term light curves

Band	NGC 3227		NGC 5506	
	$A/10^{-2}$	rms	$A/10^{-2}$	rms
2-10 keV	1.93 ± 0.06	46%	0.73 ± 0.04	24%
3-5 keV	2.24 ± 0.08	50%	0.69 ± 0.04	26%
7-15 keV	1.54 ± 0.05	38%	0.72 ± 0.04	22%

power-law model, the interpretation of the normalisation A is dependent on the low-frequency slope. For low-frequency slopes of -1 in the bending power-law model, the normalisation A can be simply interpreted as the maximum value reached by the power in a plot of frequency \times power. In this case, there is equal light curve variance per decade of frequency over the slope = -1 portion of the PSD, with the fractional variance per decade (i.e. absolute variance normalised by mean-squared) $\sigma_{\text{frac}}^2 \simeq 2.3A$. The PSDs of both AGN are consistent with this shape of low-frequency PSD, so we simply fit the best-fitting 2-10 keV bending power-law PSD model for each AGN to all energy bands, and use the spread in normalisations fitted to $M = 10000$ simulated data sets to estimate the uncertainty in normalisation (i.e. assuming the fitted PSD model). The resulting normalisations for all energy bands are shown in Table 2, together with (for comparison) the fractional rms for the corresponding long-term monitoring light curves.

Note that for each individual source the variations in fractional rms between bands is slightly larger than would be expected given the variation in normalisations (rms should scale roughly as \sqrt{A}). This is probably because the normalisation is a more robust measure of variability amplitude, since it is derived by the PSD fit across a broad frequency range, with the method taking account of the effects of the weakly non-stationary nature of the light curves. However, there are large variations in PSD normalisation between energy bands in NGC 3227, with PSD normalisation decreasing towards higher energies. In contrast, the PSD normalisation of NGC 5506 shows no significant variation with energy. Interestingly, there is also a large systematic differ-

ence between the PSD normalisations of the two AGN, with NGC 3227 showing a PSD normalisation a factor ~ 2.6 larger than the PSD normalisation of NGC 5506.

5 DISCUSSION

We first recap the main results of our Monte-Carlo analysis of the PSDs of NGC 3227 and NGC 5506, which are:

(i) The 2-10 keV PSDs of NGC 3227 and NGC 5506 are consistent with a bending power-law model similar to that observed in the high/soft state of Cyg X-1 and the NLS 1 NGC 4051, with a low-frequency slope of -1, similar bend frequencies of a few 10^{-5} Hz, and slopes steeper than -2 above the bend.

(ii) A doubly-broken power-law PSD shape, with a ratio of high to low break frequencies of 10-30, similar to that observed in the low/hard state for Cyg X-1, is rejected at better than 95 per cent confidence in NGC 3227, but is an acceptable description of the PSD of NGC 5506.

(iii) The 3-5 keV and 7-15 keV PSDs of both AGN are consistent with having the same shape as the 2-10 keV PSD, although there is a tendency for the lower energy PSD fits to prefer a lower bend-frequency and steeper slope, suggesting relatively less high-frequency power than in the harder band, consistent with the energy dependence of PSD shape in other AGN. In NGC 3227 PSD normalisation in the 3-5 keV band is nearly 50 per cent larger than in the 7-15 keV band, while there is no significant difference in normalisation between bands in NGC 5506.

(iv) In all bands the PSD normalisation of NGC 3227 is more than a factor 2 greater than that of NGC 5506.

We now examine the implications of our results for the nature of the X-ray variability of our two targets and of Seyfert galaxies in general.

5.1 PSD characteristic time-scales

To compare the PSD characteristic time-scales observed in NGC 3227 and NGC 5506 with those of other AGN, we will use the break-frequencies obtained from the sharply broken PSD models which have been used to fit most AGN PSDs so far [e.g. Markowitz et al. (2003)]. We convert the frequencies into time-scales and tabulate the results so far obtained for AGN with observed (or at least well-constrained) PSD breaks in Table 3. We also include the best estimates so far of black hole masses, and bolometric luminosity as a fraction of Eddington luminosity for these AGN. We plot black hole mass versus PSD break time-scale in Fig. 11. A similar plot is shown in M^cHardy et al. (2005), and we use the same values of black hole masses here. Most of the masses are estimated using optical reverberation mapping (shown as filled circles in the plot), but some (shown as open circles) are obtained using other methods such as stellar velocity dispersion [i.e. Mrk 766, MCG-6-30-15 and NGC 5506 (where we use the stellar velocity dispersion measurement of ~ 180 km s⁻¹ (Oliva et al., 1999), to infer a black hole mass of $\sim 10^8 M_{\odot}$ (Ferrarese & Merritt, 2000; Gebhardt et al., 2000; Ferrarese et al., 2001; Wandel, 2002)), O[III] line width (Akn 564) and a water maser measurement in the case of NGC 4258 and a range of methods for NGC 4395. Detailed references

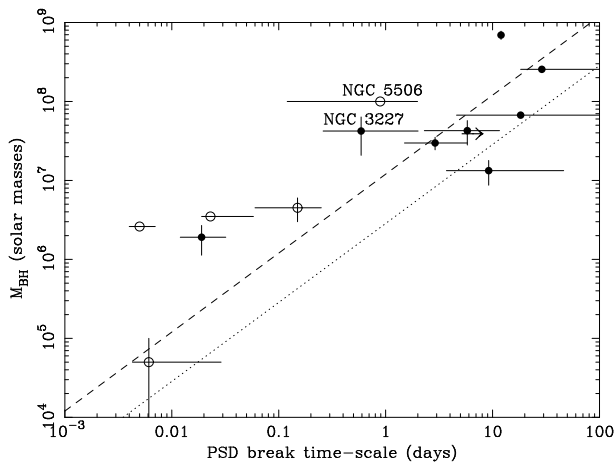


Figure 11. Black hole mass versus PSD break time-scale. Points with masses determined from optical reverberation mapping are marked by filled circles, while open circles mark points with masses determined using other methods. The arrow denotes the lower-limit on the NGC 4258 break time-scale (Markowitz & Uttley, 2005). The straight lines represent the expected relations if linear scaling is assumed from the typical break time-scales observed in the high/soft and low/hard states of Cyg X-1 (dashed and dotted lines respectively), assuming a $10 M_{\odot}$ black hole in this BXR. See text and M^cHardy et al. (2005) for further details.

are provided in Table 3. We also plot the mass-time-scale relations expected from a linear extrapolation from typical break time-scales observed in the black hole candidate Cyg X-1 in its low/hard and high/soft states^{††} (assuming a $10 M_{\odot}$ black hole in Cyg X-1).

Despite the different methods used to estimate black hole mass, it is worth noting that the data points which lie systematically above the high/soft state line (i.e. with shorter break time-scales than expected) consist of both reverberation-mapped and non-reverberation-mapped AGN. M^cHardy et al. (2004, 2005) have suggested that the deviation from linear scaling with Cyg X-1 may be a function of accretion rate. We examine this possibility in Fig. 12, which shows the ratio of the observed PSD break time-scale to that expected from linear scaling with the high/soft state break time-scale in Cyg X-1, versus the ratio of bolometric luminosity, L_{bol} to the Eddington rate for the given black hole mass ($L_{\text{Edd}} = 1.26 \times 10^{38} \text{ erg s}^{-1} M_{\odot}^{-1}$), which is a proxy for the accretion rate (in Eddington units), assuming a constant efficiency. The bolometric luminosities are obtained from the literature and are generally estimated by integrating the available spectral energy distributions of the AGN (see Table 3 for references). However, since no such estimates exist for Mrk 766 or NGC 5506, we estimated the bolometric luminosity by applying a bolometric correction factor of 36.6 to the 2-10 keV X-ray luminosities^{†††} (the 2-10 keV X-ray luminosity of NGC 5506 is estimated using the

^{††} We assume a break-frequency of 3.3 Hz in the low/hard state (e.g. see UMP02), and 13.9 Hz in the high/soft state (M^cHardy et al., 2004)

^{†††} We estimate this correction factor by assuming the monochromatic 2 keV correction factor of Padovani & Rafanelli (1988) and

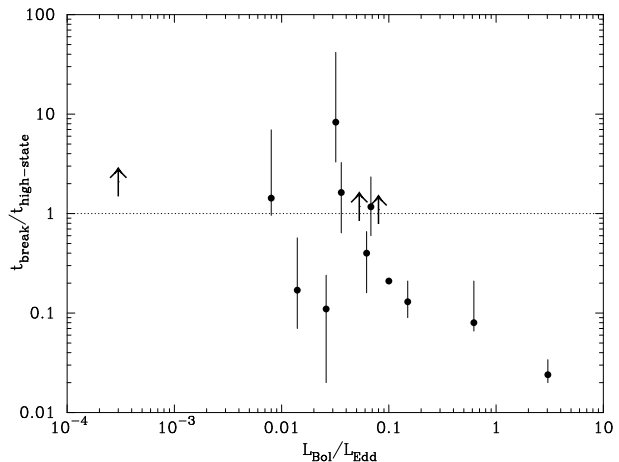


Figure 12. Ratio of the observed PSD break time-scale to that expected from linearly scaling the break time-scale of 13.9 Hz observed in Cyg X-1 in the high/soft state by the AGN black hole mass, versus the ratio of bolometric to Eddington luminosity (i.e. a proxy for accretion rate). Arrows mark lower limits on the break-time-scale ratio. See text for further details.

RXTE data, while for Mrk 766 it is obtained from Pounds et al. (2003)).

There does appear to be an overall trend for higher accretion rate AGN to show shorter break time-scales, in agreement with the hypothesis of M^cHardy et al. (2004). However, NGC 3227 and NGC 5506 show break time-scales systematically shorter than other AGN of similar mass and accretion rate. Note that the errors due to uncertainty in the mass are not accounted for in the Figure. Since mass affects both L_{Edd} and the break time-scale ratio, the errors on both axes are correlated: if the assumed mass is increased, data points move proportionately down and to the left, if it is decreased, data points move up and to the right. In this way, NGC 3227 and NGC 5506 could be made more consistent with the other AGN if the current masses for NGC 3227 and NGC 5506 are overestimated. However, it seems unlikely that all the AGN data points can be made consistent with a single break-time-scale ratio in this way, because to do so would require making a high accretion-rate AGN such as Ark 564 even more super-Eddington than is already implied by its small black hole mass. Cyg X-1 transitions to the high/soft state at $L_{\text{bol}} \simeq 0.03 L_{\text{Edd}}$ (Maccarone, 2003), and its bolometric luminosity does not seem to increase much above this value (e.g. see Zhang et al. 1997). Thus if Cyg X-1 in the high/soft state were placed on the same plot as the AGN (at a break time-scale ratio of 1, by construction), it would be consistent with the AGN data points at similar accretion rates.

5.2 PSD Normalisations

The different energy-dependence of PSD normalisations in NGC 3227 and NGC 5506 may result from the presence of different constant emission components in these sources, or intrinsically different spectral variability. For example if the

integrating over the 2-10 keV range assuming a typical photon index $\Gamma = 2$.

Table 3. PSD break time-scales, masses and accretion rates

Target	PSD break time-scale (d)	Ref	M_{BH} / $10^6 M_{\odot}$	Ref	$L_{\text{bol}}/L_{\text{Edd}}$	Ref
Fairall 9	$28.9^{+\infty}_{-10.6}$	M03	255 ± 56	P04	0.053	W02
NGC 5548	$18.3^{+\infty}_{-13.7}$	M03	67.1 ± 2.6	P04	0.080	W02
NGC 4151	$9.2^{+37}_{-5.5}$	M03	13.3 ± 4.6	P04	0.032	W02
PG 0804+761	12	P03	693 ± 83	P04	0.10	W02
NGC 3516	$5.8^{+5.8}_{-3.5}$	M03	42.7 ± 14.6	P04	0.036	W02
NGC 3783	$2.9^{+2.9}_{-1.4}$	M03	29.8 ± 5.4	P04	0.068	W02
NGC 5506	$0.89^{+1.1}_{-0.77}$	this work	100	O99	0.026	XBC
NGC 3227	$0.59^{+1.42}_{-0.33}$	this work	42.2 ± 21.4	P04	0.014	W02
MCG-6-30-15	$0.15^{+0.10}_{-0.09}$	M05	4.5 ± 1.5	M05	0.062	R97
Mrk 766	$0.023^{+0.035}_{-0.004}$	V03	3.5	B05	0.62	XBC
NGC 4051	$0.019^{+0.013}_{-0.007}$	M04	1.91 ± 0.78	P04	0.15	W02
NGC 4395	$0.006^{+0.023}_{-0.002}$	V04	$0.05^{+0.05}_{-0.04}$	V04	0.008	L99
Akn 564	$0.005^{+0.002}_{-0.001}$	P02	2.6 ± 0.26	B04	3.04	R04
NGC 4258	$513^{+\infty}_{-508}$	M05	$39.0^{+1.0}_{-1.0}$	H99	$< 3 \times 10^{-4}$	L96

References used for break time-scales: M03 - Markowitz et al. (2003); M04 - McHardy et al. (2004); M05 - McHardy et al. (2005); MU05 - Markowitz & Uttley (2005); P02 - Papadakis et al. (2002); P03 - Papadakis, Reig & Nandra (2003) (note that no error is quoted for the break time-scale of PG 0804+761 by Papadakis, Reig & Nandra (2003)); V03 - Vaughan & Fabian (2003); V04 - Vaughan et al. (2004). References used for black hole masses: B04 - Botte et al. (2004); B05 - Botte et al. (2004); H99 - Herrnstein et al. (1999); M05 - McHardy et al. (2005); O99 - Oliva et al. (1999); P04 - Peterson et al. (2004); V04 - Vaughan et al. (2004). References used for $L_{\text{bol}}/L_{\text{Edd}}$: L96 - Lasota et al. (1996); L99 - Lira et al. (1999); R04 - Romano et al. (2004); R97 - Reynolds et al. (1997); W02 - Woo & Urry (2002); XBC - assuming factor 36.6 bolometric correction from 2–10 keV X-ray luminosity (see text for details).

spectral shape of the variable continuum is not itself intrinsically variable, a constant component with a harder spectrum than the variable continuum component could dilute the fractional amplitude of variability at harder energies, to produce an overall reduction in PSD amplitude with increasing energy, as observed in NGC 3227. Evidence for constant hard components can be seen in several other AGN, including NGC 5506, using the ‘flux-flux plot’ method of spectral analysis (Taylor, Uttley & McHardy 2003, see also Vaughan & Fabian 2004). In NGC 5506, this constant component, which may be associated with disk reflection in other AGN (Fabian & Vaughan, 2003; Vaughan & Fabian, 2004), is relatively weak, which might explain the weak energy dependence of the PSD normalisation in this source. Consistent with this possibility, Bianchi et al. (2003) find no evidence for an accretion disk reflection component in the X-ray spectrum of NGC 5506. Note that, since any constant component in NGC 5506 is probably weak, the relatively small PSD normalisation observed in NGC 5506 compared to NGC 3227 is likely to be intrinsic to the varying continuum, and not simply due to dilution by constant components of different strength.

It is possible that the much stronger energy-dependence of the PSD normalisation observed in NGC 3227 is due to a stronger constant reflection component in this source. To check this possibility, in Fig. 13 we show a flux-flux plot (see Taylor, Uttley & McHardy (2003) for details of the method) for NGC 3227, made with the 3–5 keV and 7–15 keV monitoring data used here (but excluding the period four months on either side of the peak absorption of the 2001 event). Unlike the NGC 5506 data, which is well fitted by a linear plus constant model (see Taylor, Uttley & McHardy 2003), the NGC 3227 data is best fitted with a power-law of index 0.77 ± 0.02 ($\chi^2 = 11.8$ for 8 degrees of freedom) with no constant component required. As shown by Taylor, Uttley & McHardy (2003), this simple power-law description of the

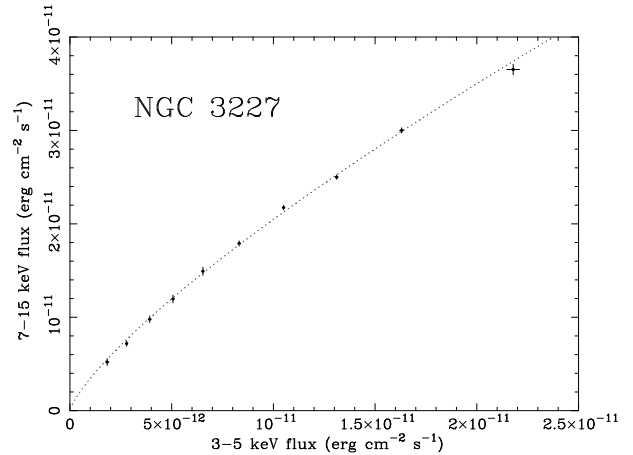


Figure 13. Flux-flux plot of NGC 3227, created by binning individual 7–15 keV flux measurements according to their 3–5 keV flux (see Taylor, Uttley & McHardy (2003) for more details of the method). The dotted line shows the best-fitting power-law model (see text for details).

flux-flux plot corresponds to intrinsic spectral pivoting of the varying continuum about an energy of a few hundred keV. Therefore the energy dependence of PSD normalisation in NGC 3227 is intrinsic to the varying continuum, and not caused by a constant hard component. In other words, the flux changes (at least on long time-scales) observed in all bands are caused primarily by the pivoting of the continuum, with the relatively larger changes at softer energies being a natural result of this effect.

It is interesting to note that if the flux variability observed in NGC 3227 results largely from spectral pivoting, the variations in the total luminosity integrated to high energies should be less than the variations we observe. We note that NGC 4051 also shows spectral pivoting (Taylor, Uttley

& M^cHardy, 2003; Uttley et al., 2004) and a relatively large amplitude of variability compared to other AGN (M^cHardy et al., 2004). It is possible that these large amplitude variations may simply be an effect of the spectral pivoting, combined with the relatively low, 2-10 keV energy band which we use to observe the varying continuum. The total X-ray luminosity variations in these AGN may not be much different from those in other AGN, in which case the explanation for the observed differences may lie with the origin of spectral pivoting. Zdziarski et al. (2002) point out that spectral pivoting can arise when the variability is driven by seed photons from the disk, which Compton-cool the corona. On the other hand, if the variability is driven mainly by variations in the corona itself, feedback effects due to disk heating may lead to a constant spectral shape. Therefore the energy dependence and amplitude of PSD normalisation may give clues to the ultimate origin of the variability, either in the disk or the corona. For completeness, we also note that gravitational light bending models suggested to explain the weak variability of the reflection component in MCG-6-30-15 and other AGN (Miniutti & Fabian, 2004), could also produce behaviour in a flux-flux plot which mimics spectral pivoting (see Fabian et al. 2004). For this model to apply in NGC 3227 however, the reflection component would need to be well hidden (e.g. strongly smeared out), since no evidence for a broad iron line feature is seen in the X-ray spectrum, even at low continuum flux levels (e.g. Lamer et al. 2003), where the equivalent width of such features is greatest in light bending models (Miniutti & Fabian, 2004).

Finally, we point out that the observed PSD normalisations of NGC 5506 and NGC 3227 bracket the PSD normalisation of Cyg X-1 (which is 0.012 in the 8-13 keV band which is undiluted by the constant thermal emission, M^cHardy et al. 2004^{§§}). The range of AGN PSD normalisations appears to be intrinsic to the variability process, and not simply due to the presence of constant components of different strengths. It is not yet clear whether the PSD normalisation is correlated with parameters such as accretion rate or black hole mass, although the similarity between the long-term variability amplitudes of NGC 4051 and NGC 3227 (with very different spectral shapes, masses and accretion rates) would suggest that it isn't. Therefore, after taking account of stochastic variations, some of the scatter in relations between short-term variability and optical line width (Turner et al., 1999), or black hole mass (Papadakis, 2004; Nikolajuk, Papadakis & Czerny, 2004) may be due to intrinsic differences in PSD normalisation, caused by some currently unknown mechanism.

5.3 NGC 3227: a high/soft state PSD in a hard-spectrum, broad-line AGN?

It is commonly assumed that NLS 1 are analogous to BHXRBs in the high/soft or very high states, whereas 'normal' broad line Seyferts are compared with the low/hard state. NGC 3227 shows that this assumption is too simplistic, at least with regard to using the variability as a diag-

nostic of the 'state'. There may indeed be a tendency for NLS 1 to show high/soft state PSDs (e.g. NGC 4051 is the best example to date, (M^cHardy et al., 2004)), but broad line Seyferts can also show high/soft state PSDs. This is not surprising, since the transition from the low/hard to high/soft state in BHXRBs occurs on average at about 2 per cent of the Eddington luminosity (Maccarone, 2003), similar to the Eddington fraction estimated for NGC 3227, assuming the reverberation-mapped mass of $\sim 4 \times 10^7 M_{\odot}$ (Peterson et al., 2004). In fact, many nearby broad line AGN exceed this Eddington fraction (e.g. see Table 3 in Wandel, Peterson & Malkan 1999), so it is likely that many luminous broad line AGN are found in the high/soft or very high states.

The analogy of NLS 1 with the high/soft state in BHXRBs is made because both NLS 1 and high/soft state BHXRBs typically show steep power-law continuum spectra, with photon indices $\Gamma > 2$ (McClintock & Remillard, 2005; Brandt, Mathur & Elvis, 1997). However, NGC 3227 shows an intrinsically hard continuum with photon index $\Gamma \sim 1.6$ (Lamer, Uttley & M^cHardy, 2003), saturating at ~ 1.8 at high fluxes [c.f. NGC 4051 which saturates at $\Gamma \sim 2.4$ (Lamer et al., 2003)], with its flux-flux plot showing no evidence for additional strong reflection which would flatten an otherwise steep primary continuum. Therefore, the variability of NGC 3227 demonstrates that continuum spectral shape and PSD shape are not simply correlated. A source may show a high/soft state PSD together with a low/hard state X-ray spectrum.

6 CONCLUSIONS

We have used X-ray monitoring of the Seyfert galaxies NGC 3227 and NGC 5506 over a broad range of time-scales to construct broadband PSDs for these AGN, and demonstrated that both PSDs are consistent with being the same shape as PSDs of BHXRBs in the high/soft state. We further rule out the possibility of a low/hard state PSD in NGC 3227, so that, together with MCG-6-30-15 (M^cHardy et al., 2005), it represents the second clear example (after NGC 4051) of a high/soft state PSD in an AGN. The normalisation of the PSD of NGC 3227 is significantly larger than that of NGC 5506, and unlike NGC 5506, NGC 3227 shows a strong energy dependence of PSD normalisation, with greater variability at lower energies. Both the energy dependence of normalisation and the large variability amplitude may be a result of spectral pivoting of the power-law continuum of NGC 3227 at high energies, also similar to NGC 4051. However, the main result to come out of this work is the fact that NGC 3227, *unlike NGC 4051* is a broad line Seyfert 1.5 with an intrinsically hard X-ray spectrum, yet it has a broadband X-ray variability PSD reminiscent of BHXRBs in the high/soft state. The combination of a low/hard-state-like X-ray spectrum with a PSD reminiscent of the high/soft state suggests that the current nomenclature for the various states is inappropriate. Therefore it may be necessary to refer to separate variability and spectral states, which are connected in some complex but as yet unknown way.

^{§§} We note here that due to a typographical error the values of normalisation shown for 8-13 keV in Tables 1-4 of M^cHardy et al. (2004) are a factor 10 too low

Acknowledgments

This research has made use of data obtained from the High Energy Astrophysics Science Archive Research Center (HEASARC), provided by NASA's Goddard Space Flight Center. PU acknowledges support from PPARC and current support from the US National Research Council. IM^cH acknowledges the support of a PPARC Senior Research Fellowship.

References

- Belloni T., Hasinger G., 1990, *A&A*, 227, L33
 Bianchi S., Balestra I., Matt G., Guainazzi M., Perola G.C., 2003, *A&A*, 402, 141
 Botte V., Cirotti S., Rafanelli P., Di Mille F., 2004, *AJ*, 127, 3168
 Botte V., Cirotti S., Di Mille F., Rafanelli P., Romano A., 2005, *MNRAS*, 356, 789
 Brandt W. N., Mathur S., Elvis M., 1997, *MNRAS*, 285, L25
 Churazov E., Gilfanov M., Revnivtsev M., 2001, *MNRAS*, 321, 759
 Done C., Madejski G. M., Mushotsky R. F., Turner T. J., Koyama K., Kunieda H., 1992, *ApJ*, 400, 138
 Edelson R., Nandra K., 1999, *ApJ*, 514, 682
 Fabian A. C., Vaughan S., 2003, *MNRAS*, 340, L28
 Fabian A. C., Miniutti G., Gallo L., Boller Th., Tanaka Y., Vaughan S., Ross R. R., 2004, *MNRAS*, 353, 1071
 Ferrarese L., Merritt D., 2000, *ApJ*, 539, L9
 Ferrarese L., Pogge R. W., Peterson B. M., Merritt D., Wandel A., Joseph C. L., 2001, *ApJ*, 555, L79
 Gebhardt K., et al., 2000, *ApJ*, 539, L13
 Green A. R., McHardy I. M., Lehto H. J., 1993, *MNRAS*, 265, 664
 Herrnstein J. R., 1999, *Nature*, 400, 539
 Lamer G., Uttley P., McHardy I. M., 2003, *MNRAS*, 342, L41
 Lamer G., McHardy I. M., Uttley P., Jahoda K., 2003, *MNRAS*, 338, 323
 Lasota J.-P., Abramowicz M. A., Chen X., Krolik J., Narayan R., Yi I., 1996, *ApJ*, 462, 142
 Leighly K. M., 1999, *ApJS*, 125, 297
 Lira P., Lawrence A., O'Brien P., Johnson R. A., Terlevich R., Bannister N., 1999, *MNRAS*, 305, 109
 Maccarone T. J., 2003, *A&A*, 409, 697
 McClintock J. E., Remillard R. A., 2005, to appear in W. H. G. Lewin, M. van der Klis eds., *Compact Stellar X-ray Sources*, Cambridge University Press, Cambridge (astro-ph/0306213)
 McHardy I. M., 1988, *Mem. Soc. Astron. Ital.*, 59, 239
 McHardy I. M., Papadakis I. E., Uttley P., Page M. J., Mason K. O., 2004, *MNRAS*, 348, 783
 McHardy I. M., Gunn K. F., Uttley P., Goad M. R., 2005, *MNRAS*, 359, 1469
 Markowitz A. et al., 2003, *ApJ*, 593, 96
 Markowitz A., Uttley P., 2005, *ApJ*, 625, L39
 Miniutti G., Fabian A. C., 2004, *MNRAS*, 349, 1435
 Murphy E. M., Lockman F. J., Laor A., Elvis M., 1996, *ApJS*, 105, 369
 Nagar N. M., Oliva E., Marconi A., Maiolino R., 2002, *A&A*, 391, L21
 Nandra K., Papadakis I. E., 2001, *ApJ*, 554, 710
 Nikolajuk M., Papadakis I. E., Czerny B., 2004, *MNRAS*, 350, L26
 Nowak M. A., Vaughan B. A., Wilms J., Dove J. B., Begelman M. C., 1999, *ApJ*, 510, 874
 Nowak M. A., 2000, *MNRAS*, 318, 361
 Oliva E., Origlia L., Maiolino R., Moorwood A. F. M., 1999, *A&A*, 350, 9
 Onken C. A., Peterson B. M., Dietrich M., Robinson A., Salamanca I. M., 2003, *ApJ*, 585, 121
 Padovani P., Rafanelli P., 1988, *A&A*, 205, 53
 Papadakis I. E., 2004, *MNRAS*, 348, 207
 Papadakis I. E., Brinkmann W., Negoro H., Gliozzi M., 2002, *A&A*, 382, L1
 Papadakis I. E., Reig P., Nandra K., 2003, *MNRAS*, 344, 993
 Peterson B. M., et al., 2004, *ApJ*, 613, 682
 Pottschmidt K. et al., 2003, *A&A*, 407, 1039
 Pounds K. A., Reeves J. N., Page K. L., Wynn G. A., O'Brien P. T., 2003, *MNRAS*, 342, 1147
 Reig P., Papadakis I., Kylafis N. D., 2002, *A&A*, 382, 202
 Reynolds C. S., Ward M. J., Fabian A. C., Celotti A., 1997, *MNRAS*, 291, 403
 Romano P., et al., 2004, *ApJ*, 602, 635
 Shemmer O., Uttley P., Netzer H., McHardy I. M., 2003, *MNRAS*, 343, 1341
 Taylor R. D., Uttley P., McHardy I. M., 2003, *MNRAS*, 342, L31
 Turner T. J., George I. M., Nandra K., Turcan D., 1999, *ApJ*, 524, 667
 Uttley P., McHardy I. M., Papadakis I. E., 2002, *MNRAS*, 332, 231 (UMP02)
 Uttley P., Taylor R. D., McHardy I. M., Page M. J., Mason K. O., Lamer G., Fruscione A., 2004, *MNRAS*, 347, 1345
 Vaughan S., Fabian A. C., 2003, *MNRAS*, 341, 496
 Vaughan S., Fabian A. C., Nandra K., 2003a, *MNRAS*, 339, 1237
 Vaughan S., Edelson R., Warwick R. S., Uttley P., 2003b, *MNRAS*, 345, 1271
 Vaughan S., Fabian A. C., 2004, *MNRAS*, 348, 1415
 Vaughan S., Iwasawa K., Fabian A. C., Hayashida K., 2004, *MNRAS* in press (astro-ph/0410261)
 Wandel A., 2002, *ApJ*, 565, 762
 Wandel A., Peterson B. M., Malkan M. A., 1999, *ApJ*, 526, 579
 Woo J.-H., Urry C. M., 2002, *ApJ*, 579, 530
 Zdziarski A. A., Poutanen J., Paciesas W. S., Wen L., 2002, *ApJ*, 578, 357
 Zhang S. N., Cui W., Harmon B. A., Paciesas W. S., Remillard R. E., van Paradijs J., 1997, *ApJ*, 477, L95

This paper has been produced using the Royal Astronomical Society/Blackwell Science L^AT_EX style file.